21st Australasian Fluid Mechanics Conference
Adelaide, Australia
10-13 December 2018

# Experimental investigation into turbulent negatively buoyant jets using combined PIV and LIF measurements

**L. M. McGurk, N. Williamson, S. W. Armfield and M. P. Kirkpatrick**

School of Aerospace, Mechanical and Mechatronic Engineering
The University of Sydney, NSW 2006, Australia

## Abstract

Turbulent negatively buoyant jets occur when the buoyancy of a jet opposes its source momentum. In these flows, the fluid will rise until it reaches a stagnation point where it changes direction and a return flow is established, forming a fountain [3]. This study looks at both the initial negatively buoyant jet stage of this flow, before the return flow has established, and the fully developed fountain stage. Two-dimensional planar particle image velocimetry (PIV) and laser induced fluorescence (LIF) are used to simultaneously measure the velocity and scalar concentration fields. The flow is investigated experimentally using a $1\text{m}^3$ tank and salt-water/freshwater negatively buoyant jets, allowing for measurements to be taken at $Fr = 58$ and $Re = 6400$. The entrainment coefficient for a negatively buoyant jet has been estimated as $\alpha \approx 0.047$, lower than a neutral jet at $\alpha \approx 0.051$. A finding consistent with existing literature [1, 6]. For a fully developed fountain, $\alpha$ corresponding to entrainment from the return flow into the inner-flow has been estimated as $\alpha \approx 0.044$, indicating entrainment into the inner-jet region is reduced with the presence of a return flow.

## Introduction

A vertically aligned turbulent round jet with negative buoyancy will rise from its source due to its initial momentum. Opposing buoyancy forces eventually reduce the momentum of the jet to zero where the fluid changes direction and forms an annular return flow. The period prior to the return flow forming will be referred to as the 'negatively buoyant jet' stage. After this initial rise the return flow starts to interact with the upward-flowing fluid, ultimately reducing the initial height of the jet, $z_i$, to a final 'quasi steady-state' height, $z_{ss}$, which the flow oscillates around indefinitely. This stage of the flow is distinctly different from the negatively buoyant jet stage and will be referred to as the 'fully developed fountain' stage. For high Reynolds numbers, the mean and steady state rise heights are governed by the Froude number,

$$Fr_o = \frac{u_o}{\sqrt{r_o g_o^{'}}}, \tag{1}$$

where $u_o$ is the vertical velocity, $r_o$ is the radius of the inlet and $g_o^{'} = g(\rho_o - \rho_a)/\rho_a$ is the 'reduced gravity' (with subscript $o$ indicating values are taken at the source) [3]. Here $\rho_o$ and $\rho_a$ are the densities of the source and ambient fluid respectively and $g$ is the gravitational acceleration. It has been shown that $z_{ss} = 2.46Fr$ for fountains with $Fr \gtrsim 5.5$ [3].

The classical plume model by Morton, Taylor and Turner [7] has underpinned many attempts to model negatively buoyant jets. These use the conservation of mass, momentum and buoyancy equations, coupled with the 'entrainment assumption', to produce integral models to predict the flow. The entrainment assumption states that the the radial velocity, $v$, of fluid moving from the ambient into a plume/jet is proportional to a characteristic vertical velocity at that height, $u$, often taken as the centreline velocity [7]. The constant of proportionality, the 'entrainment coefficient', is denoted $\alpha$ and is usually assumed to remain constant with distance from the source. There has been considerable work applying these integral models to neutral/positively buoyant jets and plumes, with estimates in literature for the entrainment coefficient spanning the ranges $0.047 \lesssim \alpha_j \lesssim 0.060$ for pure jets and $0.074 \lesssim \alpha_p \lesssim 0.11$ for pure plumes (for Gaussian velocity and buoyancy profiles) [13, 5, 11]. The entrainment coefficient for buoyant jets (forced plumes) varies between these two asymptotic cases [12]. There has been considerably less consensus on the value of $\alpha$ for negatively buoyant jets, with some studies assuming the value for a neutral jet $\alpha \sim 0.06$ [1, 6] and other suggesting it may be considerably lower $\alpha \sim 0.025 - 0.039$ [10, 8]. The present research uses experimental methods to obtain measurements of the velocity and scalar concentration fields of a negatively buoyant jet and fully developed fountain. An estimate for the value of $\alpha$ for negatively buoyant jets is presented, as well as for the inner region of a fully developed fountain.

## Experiments

Negatively buoyant jets were investigated experimentally using a $1\text{m}^3$ tank filled with salt-water, with a mixture of freshwater, ethanol and Rhodamine 6G dye entering the tank as a jet from above. All experiments were performed using a round pipe of diameter $D = 5$mm as the inlet, with the exception of a single neutral jet run that used a nozzle of $D = 2$mm. Ethanol was added to freshwater in order to match the refractive index of the source fluid and the salt-water ambient, whist simultaneously achieving the desired density difference (ambient salinity of 4.49 wt.%, source ethanol content of 11.56 wt.% and $\Delta\rho/\rho = 0.0492$). The freshwater/ethanol jet is initially directed down into the salt-water ambient, and since the jet is less dense than the surroundings it eventually changes direction and returns to the free surface. Four pco.2000 CCD cameras and a double-pulsed 532nm 145mJ/pulse Evergreen Nd:YAG laser were used to obtain simultaneous planar particle induced velocimetry (PIV) and laser induced fluorescence (LIF) measurements at a frequency of 7Hz. The laser beam was shaped into a 63.5mm sheet with a thickness of $<$ 1mm in the region of interest. The flow was controlled by an Ismatic MPC-Z gear pump capable of producing a constant flow rate of up to 6L/min.

### Planar Particle Image Velocimetry (PIV)

The freshwater used in the source fluid was taken from the Sydney water supply and passed through a 'degasser' that sufficiently heated the water allowing air to escape, reducing the prevalence of bubbles. Like most city water supplies it contains many impurities, these appear as approximately $4 - 10$ pixel ($0.1 - 0.3$mm) particles on the PIV camera. For this reason, additional seeded particles were not required to obtain sufficient particle density for the PIV cross-correlation algorithm. This gave the advantage of reducing the effect of scattered light from seeded particles interfering with the LIF signal. A $532 \pm 2$nm band-pass filter was used on the lens of the PIV camera. The

PIV images were processed with aid of the PIVsuite package in MATLAB, which pre-processed the images with a min-max filter before implementing a multi-pass interrogation with a final window size of $24 \times 24$ pixels (0.78mm$\times$0.78mm).

### Planar Laser Induced Fluorescence (LIF)

Rhodamine 6G was chosen as the fluorescent dye and scalar tracer for the LIF measurements, which has a peak emission at $\sim$ 560nm [2]. The LIF camera was therefore equipped with a B+W Yellow-Orange Filter 040 that cuts off wavelengths below $\sim$ 550nm, blocking light from the particles but allowing most of the emitted light from the Rhodamine.

Despite their high power and frequency capabilities, a disadvantage of Nd:YAG lasers is that the power output can differ quite significantly ($\sim$ 10%) between pulses. The shape of the power profiles can also differ between pulses, and are not always well represented by a Gaussian curve. For these reasons an additional camera was used to obtain the laser power profile so that the pulse-by-pulse variations in power could be corrected for in each image. A 'laser calibration box' filled with the source fluid containing Rhodamine dye was placed outside of the main tank in the path of the laser sheet. It was fitted with anti-reflective coated glass on either side to minimise reflections when the laser sheet passes through and fluoresces the fluid inside. For every laser pulse captured of the flow in the main tank, this camera captured an image of the fluid inside the laser calibration box, allowing the laser power profile to be measured. Once the intensities in the main LIF image were corrected based on this profile, they were run through a wavelet based denoising algorithm designed for images taken on CCD cameras [14]. With the corrected LIF images now processed, the scalar concentration field, $C$, is then obtained by dividing the corrected image by a reference image of the maximum dye concentration. This LIF processing method was extended from Williamson et al. [16] who used the same Nd:YAG laser.

To verify this laser profile calibration and denoising procedure, a set of images of known concentration (maximum dye, $C = 1.0$) were fed into the algorithm and the scalar concentration field calculated. Three different processing methods were used so that the effect of the profile calibration and denoiser could be seen separately.

i. Standard method [16].

$$C = \frac{I - I_b}{I_c - I_b} \tag{2}$$

ii. Power profile corrected.

$$C = \frac{(I - I_b)/P}{(I_c - I_b)/P_c} \tag{3}$$

iii. Power profile corrected and images denoised with wavelet filter.

$$C = \frac{D\{(I - I_b)/P\}}{D\{(I_c - I_b)/P_c\}} \tag{4}$$

Here $I_c$ is the reference concentration image, $I_b$ is the black level background image and $I$ is the LIF image being processed. The power profile corresponding to $I$ and $I_c$ are denoted by $P$ and $P_c$, and the denoising function by $D\{\cdot\}$. The mean RMS error between the calculated and actual concentrations could then be computed for each processing test (i)-(iii), and is shown in figure 1 for a single vertical column of pixels. The error after method (i) is largest near the top of the image and decreases towards the bottom (left to right in figure 1). This could be due to the pulse-to-pulse variations in the power profile being largest towards the top of the laser sheet where the magnitude is also highest. The error in this region is reduced by $\sim$ 50% when the profile correction is implemented in method (ii), and $\sim$ 10% towards the bottom of the image. The denoising filter can be seen to further smooth out and reduce the error another $\sim$ 15%, uniformly throughout the image.

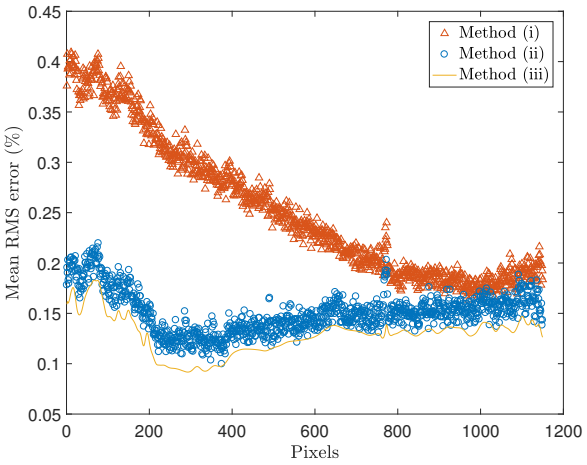


Figure 1: Mean RMS error for the scalar concentration fields of fluid of known concentration, $C = 1.0$, where the error was calculated for every pixel in a single column of the mean processed LIF image. The $\triangle$ marker corresponds to the 'standard method' (method (i)), $\circ$ corresponds to when the laser profile correction is implemented (method (ii)), and the solid line, $-$, is when the wavelet denoiser is applied (method (iii)).

## Results

PIV and LIF measurements are presented for a neutrally buoyant jet of $Re \approx 10,000$, and a negatively buoyant jet (both start up and fully developed stages) of $Re \approx 6400$ and $Fr \approx 58$. Here the Reynolds number is defined as $Re = u_o D/\nu_o$ with $\nu_o$ as the kinematic viscosity of the source mixture. The initial and steady state rise heights of the negatively buoyant jet/fountain at this Froude number are $z_i = 506$mm ($z/D = 101$) and $z_{ss} = 354$mm ($z/D = 71$). The cameras captured down-steam distances from $20 \lesssim z/D \lesssim 30$, with measurements at $z/D \approx 30$ shown in figures 2-4. The mean axial velocity, $\bar{U}$, and scalar concentration, $\bar{C}$, profiles are shown in figures 2 and 3, along with hot-wire data for a neutral jet from Hussein et al. [4], PIV/LIF results from Wang and Law [13], and laser-Doppler anemometry (LDA) and LIF results from Papanicolaou and List [9]. The horizontal axes have been normalised by the velocity and concentration profiles half-width, $r_{1/2}$, for figures 2 and 3 respectively. This is defined as the radial distance where the velocity/concentration is equal to half that at the centreline. The vertical axes have been normalised by the value at the centreline.

The present velocity results in figure 2 for the neutral jet show good agreement with Wang and Law's [13] experiments, who also used a freshwater/salt-water method with a round inlet, and reasonable agreement with Hussein et al. [4] who used a contraction/expansion inlet with an air jet. The velocity profiles for the negatively buoyant jet and fully developed fountain are similar to the neutral jet for $r/r_{1/2} \lesssim 1.5$, with the fully developed case diverging beyond this point. This difference for the fully developed fountain is expected, with negative velocities seen after $r/r_{1/2} \sim 2.0$ corresponding to the return flow. The differences between the fountain and the other cases in the region $1.5 \lesssim r/r_{1/2} \lesssim 2.0$ indicates this is where the inner jet-like flow and return flow are interacting, reducing the inner flow velocity.

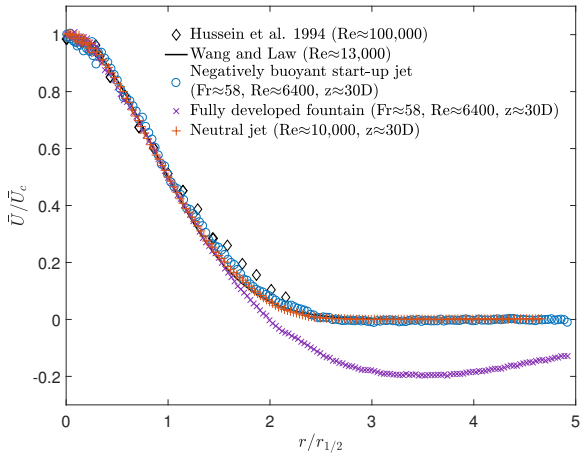


Figure 2: Velocity profiles from the present experiments for a neutral jet, $+$, a start-up negatively buoyant jet, $\circ$, and a fully developed fountain, $\times$. Experimental data from Hussein et al. [4], $\Diamond$, and the Gaussian fit from Wang and Law's [13] results, $-$, are also shown.

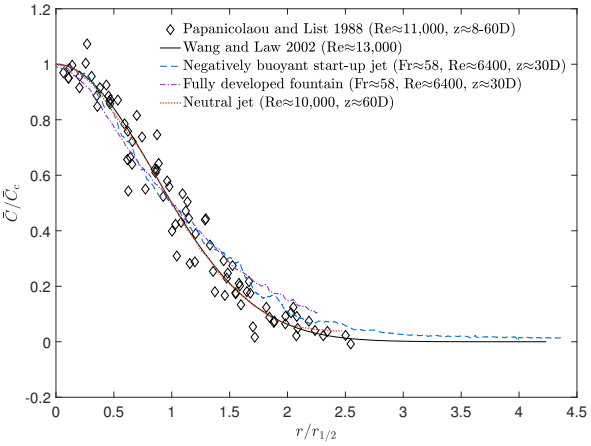


Figure 3: Scalar concentration profiles from the present experiments for a neutral jet, $\cdots$, a start-up negatively buoyant jet, $--$, and a fully developed fountain, $-\cdot-$. Neutral jet results from Papanicolaou and List [9], $\Diamond$, and a Gaussian fit from Wang and Law's [13] data, $-$, is also shown.

The present scalar concentration measurements are given in figure 3, with the neutral jet showing very close agreement with Wang and Law [13] and Papanicolaou and List's [9] results. The negatively buoyant jet and fountain differ to the neutral case, having similar scalar profiles to each other up to $r/r_{1/2} \sim 1.0$ that are both are lower than the neutral jet. Past this point they both have higher concentrations than the neutral jet but remain similar to each other until $r/r_{1/2} \sim 1.5$ where they begin to diverge. This is consistent with the velocity measurements that also show the profiles diverging at $r/r_{1/2} \sim 1.5$, which is likely due to interactions between the up-flow and return flow that are only present in the fountain case.

Figures 4(a)-(c) show the mean squared velocity fluctuations in the axial and radial directions, $\overline{u'^2}$ and $\overline{v'^2}$, and the Reynolds stress, $\overline{u'v'}$, from the present PIV measurements. The neutral jet results show good agreement with Hussein et al. [4] and Wang and Law [13] for $\overline{u'^2}$, $\overline{v'^2}$ and $\overline{u'v'}$, which are also similar to the negatively buoyant jet. The fully developed fountain shows considerably larger fluctuations and stresses throughout its width, including inside the inner jet-like region ($r \lesssim 1.5$). This implies that the turbulent mixing occurring at the inner-flow/outer-flow 'boundary' ($1.5 \lesssim r/r_{1/2} \lesssim 2.0$) still has a noticeable effect near the jet centre.

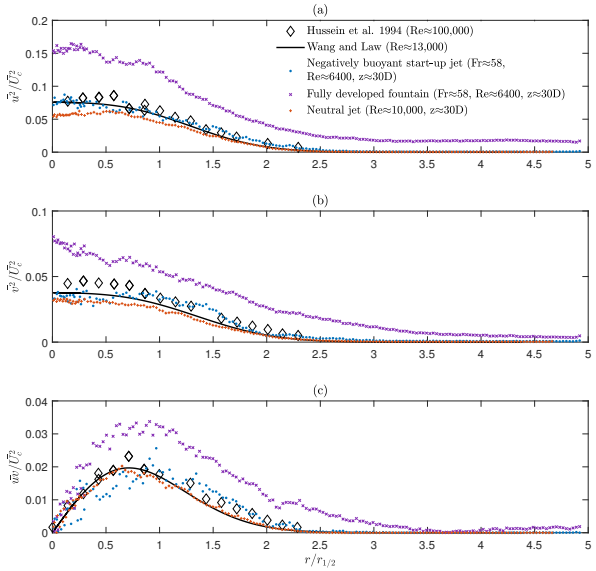


Figure 4: Present results for mean turbulent fluctuations and Reynolds stress. The neutral jet is marked with $+$, a start-up negatively buoyant jet with $\circ$, and a fully developed fountain with $\times$. Figure (a) is the mean axial velocity fluctuations, $\overline{u'^2}$, (b) is the radial fluctuations, $\overline{v'^2}$, and (c) is the Reynolds stress, $\overline{u'v'}$. Results from Hussein et al. [4] and Wang and Law [13] are shown as $\Diamond$ and $-$ respectively.

For a Bousinesq jet with self-similar velocity profiles, Hussein et al. [4] derived the following expressions to calculate the entrainment coefficient from the continuity equation

$$\alpha = \frac{I_1}{2\sqrt{2}(I_2)^{\frac{1}{2}}}, \tag{5}$$

$$I_1 = 2\int_0^\infty \left(\frac{\bar{U}}{\bar{U}_c}\right)\eta d\eta, \tag{6}$$

$$I_2 = 2\int_0^\infty \left(\frac{\bar{U}}{\bar{U}_c}\right)^2\eta d\eta, \tag{7}$$

where $\eta = r/z$ is a non-dimensional radial coordinate based on axial distance from the source. A factor of $1/\sqrt{2}$ has been added to the right hand side of (5) so that the value corresponds to Gaussian profile modelling. Using this method, the entrainment coefficient for a self-similar neutral jet, negatively buoyant jet, and fully developed fountain was calculated with distance from the source. For the fountain case, the integrals $I_1$ and $I_2$ were calculated for only the inner-jet region up to the return flow boundary (defined as when the axial velocity equals zero), where the continuity equation used to derive (5) is still valid. Figure 5 shows these results along with estimates by Hussen et al. [4] and Reeuwijk et al. [12] for a pure jet and plume. The present estimate for a neutral jet is $\alpha \approx 0.051$, which lies between Hussein et al. [4] and Reeuwijk et al.'s [12] values. The value for a negatively buoyant jet is lower, with $\alpha \approx 0.047$. This is consistent with the conclusions of Papanicolau et al. [10] and Pantzlaff and Lueptow [8] who suggested that the entrainment coefficient is reduced in jets with negatively buoyancy. The value for the inner-jet region in a fully developed fountain is lower again and estimated to be $\alpha \approx 0.044$. This value

is an estimate for $\alpha$ describing entrainment from the return-flow to the inner-flow, which has previously been assumed to be the same as for the initial negatively buoyant jet stage (corresponding to entrainment from the ambient to the jet) [1, 6]. It should be noted that equation (5) assumes self-similar flow and that the centreline velocity decays with axial distance like a jet, $\bar{U}_c = K/z$, where $K$ is a constant depending on source conditions. The present measurements support these assumptions in the region of interest investigated ($48 \lesssim z/r_o \lesssim 64$) for both negatively buoyant jets and fountains.

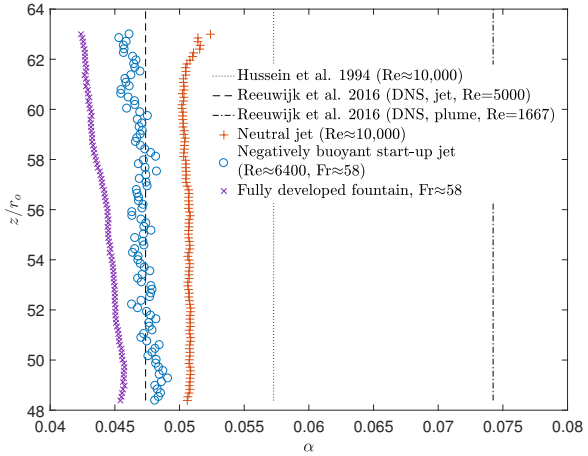


Figure 5: The entrainment coefficient, $\alpha$, for a neutral jet, $+$, negatively buoyant jet, $\circ$, and fully developed fountain, $\times$, as calculated using equation (5). The values of $\alpha$ estimated for neutral jet by Hussein et al. [4], $\cdots$, and Reeuwijk et al. [12], $--$, and for a pure plume by Reeuwijk et al. [12], $\cdot - \cdot$, are also shown.

## Conclusions

PIV and LIF measurements have been presented for a neutral jet, negatively buoyant start-up jet and fully developed fountain. A correction procedure for the LIF measurements has been discussed, which accounts for variations in power magnitude and profile shape between laser pulses. This procedure has been demonstrated to reduce errors in the concentration field by up to 50% for the present Nd:YAG laser. The profiles for velocity, scalar concentration, and turbulent fluctuations have been presented for all three jet cases. There are close similarities between the profiles of a neutral and negatively buoyant jet in the inner-jet region, $r/r_{1/2} \sim 1.0$, but these tend to slightly diverge further from the centreline. For a fully developed fountain the differences are more significant, particularly for $r/r_{1/2} \gtrsim 1.5$ but also for the inner-jet region, indicating that the presence of a return flow affects the jet even near the centreline. The entrainment coefficient has also been estimated for a negatively buoyant jet ($\alpha \approx 0.047$) and the inner region of a fully developed fountain ($\alpha \approx 0.044$), providing further evidence that entrainment is lower in negatively buoyant jets compared to neutral jets. It also suggests that when integral models are applied to fully developed fountains with a return flow, such as Bloomfield and Kerr [1] and McDougall [6], that $\alpha$ should be reduced after the initial rise once a return flow has formed.

## Acknowledgements

The support of the Australian Research Council for this project is gratefully acknowledged.

## References

[1] Bloomfield, L.J and Kerr, R.C., A theoretical model of a turbulent fountain, *J. Fluid Mech.*, **424**, 2000, 197–216.

[2] Hung, J., Castillo, J. and Olaizola, A.M., Fluorescence spectra of Rhodamine 6G for high fluence excitation laser radiation, *Journal of Luminescence*, **101**, 2003, 263–268.

[3] Hunt, G.R. and Burridge, H.C., Fountains in Industry and Nature, *Annu. Rev. Fluid Mech.*, **47**, 2015, 195–220.

[4] Hussein, J.H., Capp, S.P. and George, W.K., Velocity measurements in a high-Reynolds-number, momentum conserving, axisymmetric, turbulent jet, *J. Fluid Mech.*, **258**, 1994, 32–75.

[5] Kaminski, E., Tait, S. and Carazzo, G, Turbulent entrainment in jets with arbitrary buoyancy, *J. Fluid Mech.*, **526**, 2005, 361–376.

[6] McDougall, T.J., Negatively buoyant vertical jets, *Tellus*, **33**, 1981, 313–320.

[7] Morton, B.R., Taylor, G. and Turner, J.S., Turbulent gravitational convection from maintained and instantaneous sources, *Proc. R. Soc. Lond. A*, **234**, 1956, 1–23.

[8] Pantzlaff, L. and Lueptow, R.M., Transient positively and negatively buoyant turbulent round jets, *Experiments in Fluids.*, **27**, 1999, 117-125.

[9] Papanicolaou, P.N. and List, E.J., Investigations of round vertical turbulent buoyant jets, *J. Fluid Mech.*, **195**, 1988, 341–391.

[10] Papanicolaou, P.N., Papakonstantis, I.G. and Christodoulou, G.C., On the entrainment coefficient in negatively buoyant jets, *J. Fluid Mech.*, **614**, 2008, 447–470.

[11] Priestley, C.H.B and Ball, F.K., Continuous convection from an isolated source of heat, *Quarterly Journal of the Royal Meteorological Society*, **81, 348**, 1955, 144-157.

[12] Reeuwijk, v.M. and Craske, J., Energy-consistent entrainment relations for jets and plumes, *J. Fluid Mech.*, **782**, 2015, 333–355.

[13] Wang, H. and Law, A.W-K, Second-order integral model for a round turbulent buoyant jet, *J. Fluid Mech.*, **459**, 2002, 397–428.

[14] Weinkauff, J., Trunk, P., Frank, J.H., Dunn, M.J., Dreizler, A. and Böhm, B., Investigation of flame propagation in a partially premixed jet by high-speed-Stereo-PIV and acetone-PLIF, *Proceedings of the Compustion Institute 35*, **35, no. 3**, 2015, 3773-81.

[15] Williamson, N., Armfield, S.W. and Lin, W., Forces turbulent fountain flow behaviour, *J. Fluid Mech.*, **671**, 2011, 535–558.

[16] Williamson, N., Kirkpatrick, M.P. and Armfield, S.W., Entrainment across a sheared density interface in a cavity flow, *J. Fluid Mech.*, **836**, 2018, 999–1021.